IEEE Access
Multidisciplinary | Rapid Review | Open Access Journal

Received June 23, 2021, accepted July 22, 2021, date of publication July 27, 2021, date of current version January 12, 2022.

Digital Object Identifier 10.1109/ACCESS.2021.3100549

Pattern Descriptors Orientation and MAP Firefly Algorithm Based Brain Pathology Classification Using Hybridized Machine Learning Algorithm

B. DEEPA[1], M. MURUGAPPAN[2], (Senior Member, IEEE), M. G. SUMITHRA[3,4,5], (Senior Member, IEEE), MUFTI MAHMUD[6,7,8], (Senior Member, IEEE), AND MABROOK S. AL-RAKHAMI[9], (Member, IEEE)

[1]Department of ECE, Jayaram College of Engineering and Technology, Tiruchirappalli 621014, India
[2]Department of Electronics and Communication Engineering, Kuwait College of Science and Technology (Private University), Safat 13058, Kuwait
[3]Department of ECE, Dr. N. G. P. Institute of Technology, Coimbatore 641048, India
[4]Centre for Research and Development, Dr. N. G. P. Institute of Technology, Coimbatore 641048, India
[5]BioMedical Engineering Department, Dr. N. G. P. Institute of Technology, Coimbatore 641048, India
[6]Department of Computer Science, Nottingham Trent University, Clifton, Nottingham NG11 8NS, U.K.
[7]Medical Technologies Innovation Facility, Nottingham Trent University, Clifton, Nottingham NG11 8NS, U.K.
[8]Computing and Informatics Research Centre, Nottingham Trent University, Clifton, Nottingham NG11 8NS, U.K.
[9]Research Chair of Pervasive and Mobile Computing, Information Systems Department, College of Computer and Information Sciences, King Saud University, Riyadh 11543, Saudi Arabia

Corresponding authors: M. G. Sumithra (sumithrapalanisamy74@gmail.com), M. Murugappan (m.murugappan@gmail.com), and Mufti Mahmud (muftimahmud@gmail.com)

This work was supported by the Deanship of Scientific Research, King Saud University, through the Vice Deanship of Scientific Research Chairs.

ABSTRACT Magnetic Resonance Imaging (MRI) is a significant technique used to diagnose brain abnormalities at early stages. This paper proposes a novel method to classify brain abnormalities (tumor and stroke) in MRI images using a hybridized machine learning algorithm. The proposed methodology includes feature extraction (texture, intensity, and shape), feature selection, and classification. The texture features are extracted by intending a neoteric directional-based quantized extrema pattern. The intensity features are extracted by proposing the clustering-based wavelet transform. The shape-based extraction is performed using conventional shape descriptors. Maximum A Priori (MAP) based firefly algorithm is proposed for feature selection. Finally, hybridized support vector-based random forest classifier is used for the classification. The MRI brain tumor and stroke images are detected and categorized into four classes which are a high-grade tumor, a low-grade tumor, an acute stroke, and a sub-acute stroke. Besides, three different regions are identified in tumor detection such as edema, and tumor (necrotic and non-enhancing) region. The accuracy of the proposed method is analyzed using various performance metrics in comparison with the few state-of-the-art classification methods. The proposed methodology successfully achieves a reliable accuracy of 88.3% for classifying brain tumor cases and 99.2% for brain stroke classification. The best F-score of 0.91 and the least FPR of 0.06 are attained while considering brain tumor classification against the proposed HSVFC. Likewise, HSVFC has 0.99 as the best F-score and a 0.0 FPR in the case of brain stroke classification. The experimental analysis offers a maximum mean accuracy of different classifiers for categorizing MRI brain tumor are 76.55%, 49.24%, 65.12%, 74.36%, 69.25%,and 55.61% for HSVFC, SVM, FFNN, DC, ResNet-18 and KNN respectively. Similarly, in identifying MRI brain stroke, the average accuracy for HSVFC, SVM, FFNN, DC, ResNet-18 and KNN are 98.17%, 53.40%, 85.8%, 87.5%, 70.06%, and 61.24%, respectively is achieved.

INDEX TERMS Neoteric directional quantized extrema pattern, optimal MAP firefly algorithm, edema, necrotic and non-enhancing region.

I. INTRODUCTION

IN recent decades, the research on automatic tumors and stroke diagnosis has increased. The feature representation

The associate editor coordinating the review of this manuscript and approving it for publication was Jerry Chun-Wei Lin.

plays a salient role in high-level medical tasks like classification [1]. A tumor occurs due to the growth of the unwanted cells in an uncontrolled manner. The major brain tumor starts from the brain and has different characteristics such as size, shape, location, and image intensities [2]. The stroke happens due to the sudden interruption in the blood supply of the brain [3]. An early detection of this disease will facilitate an earlier diagnosis and increase the probability of the individual's survival. According to the World Health Organization (WHO), 15 million people across the world suffer from stroke annually. Of these, 5 million die, and another 5 million are permanently disabled. The incidence rate of stroke per year in India is between 145-154 per 1, 00,000 individuals, while that of the central nervous system (CNS) tumors ranges from 5 to 10 per 100,000 population with an increasing trend. In the United States, an estimated 23,890 adults (13,590 men and 10,300 women) were diagnosed with primary brain tumors in 2020 alone.

The above-mentioned diseases are conventionally diagnosed through medical imaging modalities such as computed tomography (CT), MRI, ultrasound scan, and positron emission tomography (PET). Among these imaging methods, MRI accurately captures the inner parts of the brain for an accurate diagnosis compared to other methods [4]. Magnetic Resonance based diffusion and perfusion analysis are more sensitive for the detection of tumors and stroke, especially in earlier stages. The precision of MRI in detecting brain tumor and stroke is attributed to its clearer vision of brain tissues obtained with the help of magnetic and radio waves.

In clinical routine, the diagnosis of brain tumor and stroke is employed by different MRI sequences such as T1-weighted (T1-w), T1-weighted with contrast enhancement (T1-wc), T2-weighted (T2-w), Proton Density-weighted (PD-w), and Fluid-Attenuated Inversion Recovery (FLAIR). T1-w is the most commonly utilized sequence for a brain tumor and it is used for simple annotation of healthy tissues. The borders of the brain tumor can be highlighted using T1-wc and this helps distinguish the active cell region and the necrotic core regions easily. The edema region can be made brighter by using the T2-w sequence. FLAIR can be observed as a highly effective sequence that helps to separate the edema region from Cerebro-Spinal Fluid (CSF) [5]. In the case of stroke, Diffusion-weighted imaging (DWI) in MRI is mostly used for detecting acute stroke. It analyses the biological tissue structure which depends on the motion of water molecules at the microscopic level [6]. By using these MRI sequences, the tasks such as feature extraction, feature selection, and classification are used for autonomously diagnose the abnormalities in the brain.

The rest of this paper is structured as follows: A detailed descriptions of the related works about the brain tumor and stroke detection and classification is provided in section II. The procedure and description of the proposed technique are explained in section III. The comparative results of the proposed technique with traditional approaches are depicted in section IV. Lastly, section V concludes the proficiency of the proposed approach.

II. RELATED WORK

Recent years have seen a sharp increase of machine learning (ML) applications in medical image analysis [7]–[17]. Out of this vast literature, particularly, in [18], the researchers have proposed an improved local derivative pattern for feature extraction. Here, the local derivative pattern variation method is used to extract the diagonal directional pattern features for brain pathology detection. Classification is carried out by a k-nearest neighbour, conventional neural network (CNN), and a support vector machine (SVM). The performance of the proposed system is limited due to time complexity. Maire *et al.* [19] presented an article by comparing nine different classification techniques using a multi-parametric MRI dataset. The high-level machine learning algorithms like Convolutional Neural Networks (CNN) and Random Decision Forests (RDF) produced significant results in classification with 77% accuracy for CNN and 82% for RDF. The limitation of this work are challenges in hyperparameter tuning and higher time complexity in training the features. A new amalgam technique in a computer-aided diagnosis (CAD) system for the detection of abnormality using MRI brain images is proposed in [20]. After a pre-processing, the features are extracted using the Gabor filter and Walsh-Hadamard transform (WHT). Finally, SVM is used for the classification of an abnormality like a tumor. The major demerit of this system is less energy compacting. In [21] the researchers utilized wavelet texture features along with several machine learning algorithms. Intensity, neighborhood information, intensity difference, and wavelet-based texture features are extracted and applied on multi-modality MRI images with numerous classifiers. The utilization of wavelet-based texture feature with random forest classifier maximizes the accuracy of classification to a rate of 81% for low-grade tumors and 85% for high-grade tumors. Automatic diagnosis and detection of stroke in DWI images are presented in [22]. The rule-based classification approach is chosen because of its simplicity and the ability to classify stroke lesions. However, the rule-based method fails to perform well to prediction quality. The analysis of DWI and FLAIR MRI images for the detection of acute stroke is presented in [23]. Three machine learning algorithms such as SVM, logistic regression, and random forest were utilized to detect an acute stroke. Though the performance of the machine learning algorithm is more feasible than human perception, it fails to detect stroke patients with small infarctions.

A new automated method to differentiate the different cancer diseases from the MRI images has been proposed in [24]. Its geometrical properties such as shape, texture, and intensity are used for classification and the results are endorsed on one local and publicly available dataset with different cross-validations on the feature set. A novel pattern descriptor referred to as a directional local quantized extrema pattern for image retrieval and indexing is presented in [25].

The standard local binary patterns and local ternary patterns encoded a greyscale relationship. This technique uses ternary patterns from Horizontal–Vertical–Diagonal–Anti diagonal structure to encode more spatial structural data to obtain better retrieval, but the assortment of features in a localized direction limits the classifier performance. Jothi *et al.* [26] have utilized a Tolerance Rough Set Firefly-based Quick Reduct (TRSFFQR) feature selection algorithm for brain tumor detection. The shape, intensity, and texture-based features are extracted from segmented images of the MRI brain. TRS and Firefly Algorithm (FA) is utilized for selecting the imperious features of a brain tumor. The results obtained from this work show that the TRS firefly-based quick redact algorithm effectively selects the useful features with substantial-quality, but the network convergence speed is slow when compared to conventional algorithms.

Automated segmentation of brain tumors in multimodal MRI images is proposed in [27]. A Fully Convolutional Neural Network (FCNN) and hand-designed features are used for the classification of MRI images. Also, random forest classification is used to classify the MRI data. This hybrid approach of machine learning feature extraction using FCNN and the proposed texture features offer better results, but it is spatially invariant to the input data. A region-based Active Contour Method (ACM) for segmentation and classification using an artificial neural network-based Levenberg-Marquardt algorithm is proposed in [28]. The process of texture and shape feature extraction helps for accurate classification. The combination of the classifier with ACM segmentation offers high accuracy (93.74%), good sensitivity (90.98%) and specificity (87.47%) measures, combined with a few shortcomings such as disability to segregate the discontinuous objects. Machhale *et al.* [29] presented an intellectual classification system, for identifying the status of the brain images by combining the SVM and KNN classifier approach. Even though the results of this hybrid approach give 98% accuracy, it requires a longer time to predict the status of the brain images if the database is larger. Gupta *et al.* [30] proposed a classification model for MRI-FLAIR images to detect a brain stroke. DWT is utilized for extracting the feature and the Principal Component Analysis (PCA) is employed for selecting the optimal features. However, the classification model achieves only 88% of accuracy and lacks time complexity. An innovative system for detecting and classifying brain tumors is described in [31]. In this system, the rougPrh set theory is developed for the process of feature extraction, and the Particle Swarm Optimization Neural Network (PSO-NN) is utilized for classifying the abnormalities in the MRI brain images. However, a large converge rate limits the performance of the classifier. Griffis *et al.* [32] have presented an approach for the automatic identification of stroke lesions by using naive Bayes classification in T1-w MRI images. The major drawback of this approach is that it is sensitive to indirect lesions which makes detection difficult. A quantitative apparent diffusion coefficient along with the relaxation time T2 in the characterizing contrast enhances the brain tumor region and the region of peritumoral edema [33]. From this, the potential value, and relationship of both Vivo quantization of the apparent diffusion coefficient along with the T2 relaxation times are investigated to characterize the cellularity of brain tumors and tumor-related edema. An intra-voxel assessment in the magnetic resonance imaging is presented in [34]. This novel technique involves a combination of various acquisitions known as intravoxel analysis which have been utilized in the evaluation of spin-spin relaxation and identification of multiple tissues. In this technique, exceedingly small number of clinical data sets are used for evaluation, which is the major disadvantage for this system.

The brain intracranial hemorrhage classification using synergic deep learning model is presented in [35]. Pre-processing is initially done using gabor filter and grab-cut based segmentation is used to identify the affected portion. Then the synergic deep learning model is utilized for extracting the features and softmax layer is used for classification. In [36], the various components of evolutionary algorithms including the fitness function, parents selection, population and crossover operators etc., for feature selection process has been discussed in detail. The fitness function forms the basis for selection of features which opens the door for improving the classifier performance by representing the task to be solved in an evolutionary context. The classification of abnormal cervical cells using transfer learning approach is depicted in [37]. ResNet50, VGG19, inception V3 and squeezeNet are utilized for abnormal cell classification. The accuracy of 97.89% is attained from ResNet50 in combination with random forest classifier for predicting the cancerous cervical cells.

III. PROPOSED METHODOLOGY

This present work aims to classify brain tumors and stroke in MRI images using hybridized machine learning algorithms. The major contributions of the proposed work is highlighted below:

- Intensity feature extraction by proposing Intensity-based Clustering Wavelet Transform (ICWT).
- Feature selection by proposing Maximum A Posteriori (MAP) based Firefly Algorithm (FFA).
- Image classification by proposing Hybridized Support Vector based Forest Classifier (HSVFC).
- Texture feature extraction by proposing Neoteric Directional based Quantized Extrema Pattern (NDQEP).

The flow diagram of the proposed methodology is shown in Figure. 1.

This hybrid machine learning framework is developed to obtain a robust model capable of handling MRI scans with hypo and hyper intense sequences. In some MRI sequences, the affected lesions appear hypo intense which makes it difficult for the radiologists to distinguish between the abnormal and the normal regions. Hence image fusion is utilized to make the lesions hyper intense in order to get better visual perception. Further, the dimension of the affected region is not predicted precisely in MRI, so image segmentation is performed to predict the exact boundary of the abnormal region.

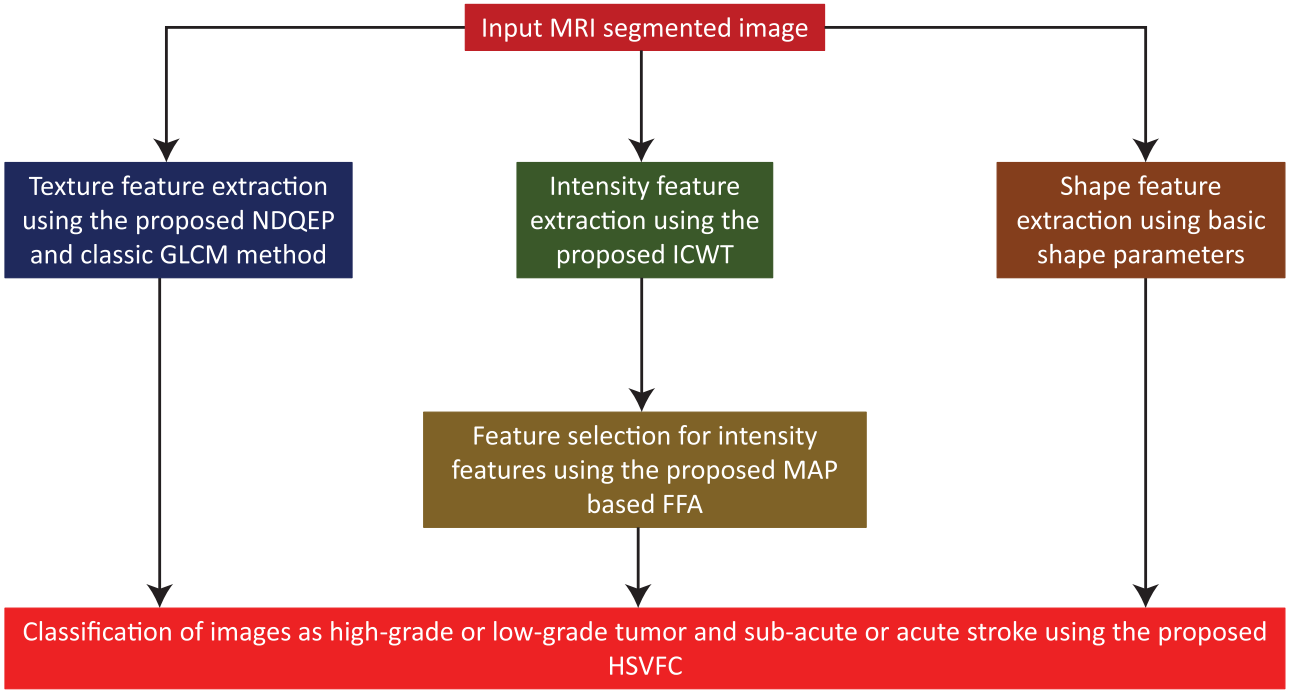

FIGURE 1. Flow diagram of the proposed methodology. Legend: NDQEP-Neoteric Directional based Quantized Extrema Pattern; GLCM - Gray Level Co-occurrence Matrix; ICWT- Intensity-based Clustering Wavelet Transform; MAP- Maximum A Posteriori; FFA- Firefly Algorithm; HSVFC- Hybridized Support Vector based Forest Classifier.

(Image fusion and segmentation is done in the previous phase of this present work which is referred in [38]). Then the texture feature extraction is carried out in the present work to extract the information from the image at various angles and to identify the various structures of the image. The intensity feature extraction is performed in this work, because the identification of different grades of tumor and stroke is based on the pixel intensity. The selection of best features is necessary to make the classification process easier and it helps the radiologist to accurately diagnose the types of tumor and stroke.

Initially, the input segmented image is taken from the earlier work, which includes image fusion and segmentation [38]. The image fusion is performed using Gradient-based Discrete Wavelet Transform (GDWT). In the fusion process, two input images are decomposed into low-frequency and high-frequency sub-bands using Discrete Haar Wavelet Transform, for which gradient and corresponding fusion rules must be applied. After fusing the images, segmentation is performed based on the Intensity Factorized Threshold (IFT) technique. Histogram equalization is performed for the fused image and matrix factorization is done to estimate the threshold for segmenting the affected region.

A. TEXTURE FEATURE EXTRACTION USING NEOTERIC DIRECTIONAL BASED QUANTIZED EXTREMA PATTERN (NDQEP)

Initially, the segmented images obtained from [38] are taken as an input for texture extraction. Then it is separated into an overlapping pattern in matrix form (Ip) with 7×7 dimensions (i.e. 49 pixels) to extract the spatial relation between any pair of neighbors in a local region along with the given directions, by varying the limit variables in each row and column index (i and j) from 1 to m-7 and 1 to n-7 respectively and is given by,

$$I_p = \lim_{i \to 1 \text{ to } (m-7), j \to 1 \text{ to } (n-7)} Seg_{ima}[a, b] \tag{1}$$

Here, 'a' indicates the indices from i^{th} row to $i + 6^{th}$ row, 'b' denotes the indices from j^{th} column to $j + 6^{th}$ column and Seg_{ima} is the segmented image obtained from our earlier work [38], m and n represents the total number of rows and columns of the segmented image (i.e 256), [.] indicates the matrix representation.

The Local Direction Extrema Values (V) in all directions are computed with dimension 7×7 by subtracting the neighbourhood pixel with the center pixel in the overlapping pattern. V is represented by,

$$V[x, y] = \lim_{x \to 1 \text{ to } 7, y \to 1 \text{ to } 7} (Ip[x, y] - Ic) \tag{2}$$

where x and y represent the scalar value for accessing row and column index of the formed pattern matrix, I_C is the center pixel of the pattern matrix. For computing the upper and lower pattern, the threshold value (th) is calculated by taking the median value for the obtained LDEV results.

Also, from the LDEV results, the multi-directional pixel value is estimated in all the different directions for extracting the upper and lower binary patterns which are shown in figure 2. Here the horizontal (0°and 180°),

vertical (90° and 270°), diagonal (45°, 135°, 225°, 315°), (30°, 60°, 120°, 150°, 210°, 240°, 300°and 330°) anti-diagonal directions are considered.

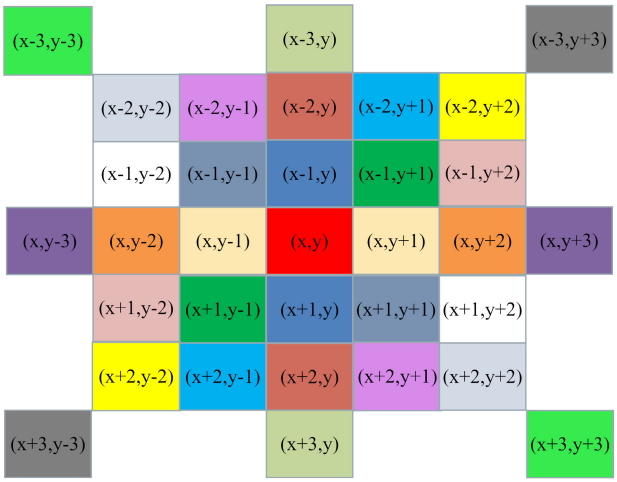

FIGURE 2. Multidirectional pixel validation.

This multi-directional pixel value representation is also called (Horizontal, Diagonal, Vertical, and Anti-diagonal) which represents the 7 × 7 matrix. In figure 2, the (x, y) signifies the row and column index of center pixel of the LDEV pattern. The $HDVA_7$ (HA_7) is calculated by the following equation,

$$HA_7 = \begin{cases} f(V45, V43, Ic); f(V46, V42, Ic); f(V47, V41, Ic); \\ \qquad \alpha = 0°\&180° \\ f(V35, V53, Ic); f(V26, V62, Ic); f(V17, V71, Ic); \\ \qquad \alpha = 45°\&225° \\ f(V34, V54, Ic); f(V24, V64, Ic); f(V14, V71, Ic); \\ \qquad \alpha = 90°\&270° \\ f(V33, V55, Ic); f(V22, V66, Ic); f(V11, V77, Ic); \\ \qquad \alpha = 135°\&315° \\ f(V23, V65, Ic); f(V32, V56, Ic); \\ \qquad \alpha = 120°, 150°, 300°\&330° \\ f(V52, V36, Ic); f(V63, V25, Ic); \\ \qquad \alpha = 30°, 60°, 210°\&240° \end{cases} \tag{3}$$

Here $f(V_{45}, V_{43}, Ic)$ signifies the $(x, y+1)^{th}$, $(x, y-1)^{th}$, $(x, y)^{th}$ locations in figure 2 respectively. Similarly, we computed all the elements using the above equation 3. As a result of equation 3, around 16 pattern pixels are formed based on the horizontal, vertical, diagonal, and anti-diagonal directions. The upper and lower binary pattern is constructed using the obtained threshold value and the multidirectional pattern pixel values which are given by,

$$f(p_1, p_2, p_3) \begin{cases} Upper_{pattern} = 1, Lower_{pattern} = 0 \quad if \\ \qquad P_1 < I_c \ and \ P_2 < I_c - th \\ Upper_{pattern} = 0, Lower_{pattern} = 1 \quad if \\ \qquad P_1 > I_c \ and \ P_2 > I_c \\ Upper_{pattern} = 0, Lower_{pattern} = 0 \quad else \end{cases} \tag{4}$$

For instance, $f(P_1, P_2, I_c)$ denoted as $f(V_{45}, V_{43}, I_c)$. This representation is repeated for all terms in equation 3. The calculated $Upper_{pattern}$ and $Lower_{pattern}$ are in array form which contains 16 binary values. Then the texture patterns for the upper and lower binary pattern are represented as:

$$UP = \sum_{b=1}^{16} Upper_{pattern}(b) * 2^{\sqrt{b}}$$
$$LP = \sum_{b=1}^{16} Lower_{pattern}(b) * 2^{\sqrt{b}} \tag{5}$$

Equation 5 provides a scalar value, where b represents the index number of pixel patterns i.e. 16 signifies the length of the formed upper and lower pattern. The attained UP and LP are replaced as the center pixel of the corresponding overlapping pattern matrix in the respective upper and lower pattern images which is expressed in equation 6.

$$Image_{lower}[i+3, j+3] = LP$$
$$Image_{upper}[i+3, j+3] = UP \tag{6}$$

Equation 2 to 6 is carried out for each overlapping pattern of the entire image. The histogram count is taken for the pattern images in equation 6 by counting the number of values that fall between 0 to $2^{\sqrt{b}}$ (i.e. vector form). Finally, the attained vectors of the counted histogram are combined to get NDQEP from which 34 features are extracted.

B. TEXTURE FEATURE EXTRACTION USING CLASSIC GRAY LEVEL CO-OCCURRENCE MATRIX (GLCM)

The image texture pattern is found by employing a pattern matrix which can be denoted as Gray Level Co-occurrence Matrix (GLCM) [39]. GLCM is a classic method in texture analysis. In this approach, the statistical parameters are extracted from the grayscale images. In this work, GLCM is utilized for extracting the texture features of the affected or abnormal region in MRI scan images. Here, the following twenty texture features are extracted from the segmented image obtained from [38]: autocorrelation, correlation I, contrast, cluster prominence, correlation II, cluster shade, energy, dissimilarity, homogeneity I, entropy, homogeneity II, sum of square, maximum probability, sum of average, sum of variance, sum of entropy, difference of entropy and difference variance, information degree of correction I and II and inverse difference normalized [40], [41].

C. SHAPE-BASED FEATURE EXTRACTION

Shape-based feature extraction plays a significant role in extracting the information from lesions in MRI scan images. The characteristics features of tumors and stroke in MRI images give more valuable information about the disease progression and its severity. In general, the size of the affected part in tumor or stroke in MRI images are larger. Hence, the following shape-based features such as area, perimeter, eccentricity, circularity, and equivdiameter [42] are extracted from the segmented images.

D. FEATURE EXTRACTION USING INTENSITY-BASED WAVELET TRANSFORM AND CLUSTERING (ICWT)

The intensity-based feature extraction can be demonstrated as the process of extracting the features based on the color intensities that help to identify the affected region of MRI brain image using intensity level. The input segmented images are separated into two sub-bands like low-frequency (L) and high-frequency (H). Then further it can be decomposed into low-low (LL), High-Low (HL), Low-High (LH), and High-high (HH) sub-band coefficients using Discrete Haar Wavelet Transform. The main objective is to extract the high-intensity features since the affected regions in the MRI brain tumor and stroke images appear with high intensity. Hence clustering concept is introduced after wavelet decomposition. The centroid value for low (L_C) and high (H_C) intensity pixels is calculated for each estimated wavelet coefficient.

$$H_C = \lim_{C \to 1 \ to \ 4} \left(\frac{max(coeff_C)}{K}\right)$$

$$L_C = \lim_{C \to 1 \ to \ 4} \left(\frac{max(coeff_C)}{K+1}\right)$$

where, $coeff_C$ *is defined as*:

$$\begin{aligned} Coeff_1 &= LL \\ Coeff_2 &= LH \\ Coeff_3 &= HL \\ Coeff_4 &= HH \end{aligned} \tag{7}$$

where C is the number of co-efficient; K is the number of pixels which is 2.

For predicting the high-intensity pixels, the cluster distance is calculated by,

$$D_H[P] = \lim_{P \to 1 \ to \ Q} \sqrt{(Coeff_C[P] - H_C)^2} \tag{8}$$

$$D_L[P] = \lim_{P \to 1 \ to \ Q} \sqrt{(Coeff_C[P] - L_C)^2} \tag{9}$$

where D_H and D_L are the high-intensity cluster distance and the low-intensity cluster distance, p denotes the index of corresponding co-efficient $coeff_C$, Q indicates the dimension of $coeff_C$. Based on cluster distance, high-intensity features are extracted and is denoted by the following equation,

$$Fea_{ICWT} = \{coeff_C[p] \quad if D_H[p] < D_L[p] \quad \forall p \in Q \tag{10}$$

E. FEATURE SELECTION USING AN OPTIMAL MAP FIREFLY ALGORITHM (MFFA)

The dimensions of the resultant ICWT features gets varied due to the variations in the affected regions of brain image among different patients. Hence to make the dimensions equal by taking the significant features, the proposed feature selection technique is utilized. The extracted ICWT features are evaluated using the fitness function. This fitness evaluation is calculated by computing the mean and variance value for every overlapping 1×8 feature, to avoid the reduction of dimensions in the optimized features. For each overlapping 1×8 features, the probability function is computed based on the Maximum A priori (MAP) approach with the help of the following equation,

$$\begin{aligned} &P(t) \\ &= \lim_{t \to \ 1 \text{ to } [size(Fea_{ICWT}-1)]} \\ &(\mu + \frac{1}{2\pi\sigma^2} * \exp(\frac{[max(Fea_{ICWT}(t), Fea_{ICWT}(t+1)) - \mu]^2}{2\sigma^2})) \end{aligned} \tag{11}$$

From the calculated probability, the optimized features are attained which is considered as population (firefly) and is given by,

$$X = \lim_{t \to 1 \ to \ [size(Fea_{ICWT})-1]} \begin{cases} \mu \quad if \quad \mu > P(t) \\ max(Fea_{ICWT}(t), \\ Fea_{ICWT}(t+1)) \quad else \end{cases} \tag{12}$$

The position of feature is considered as light intensity in the assigned population. The firefly position is updated by checking the neighborhood features and is estimated by the following equation,

$$f_d = \begin{cases} f_s(1-\beta) + \beta f_d + \alpha\epsilon \quad if \quad X(LI_d) > 0 \\ f_d \quad else \end{cases} \tag{13}$$

where f_d is the current firefly position, f_s is the previous firefly position, LI_d represents the light intensity of the current firefly, α is the adjusting parameter (i.e, 0.2), and $\epsilon = 2.220 \times 10^{-16}$is a constant. β is the estimation of attractiveness with distance r and it is given as $\beta = I_0 e^{\gamma r^2}$ and I_0 is the light intensity at the source (i.e., 1), γ is the adjusting parameter (i.e., 1), r is the distance amongst the two fireflies which is represented by $r = \sqrt{(f_s - f_d)^2}$ The above process is repeated from equation 11 to 13 until the stopping criteria is reached which occurs when the updated firefly positions at each iteration reach nearer to higher light intensity. Then, the best solution can be updated as the optimized features. As a result, two features are selected by MFFA in ICWT features.

Around 61 features are collected from feature extraction and selection for the classification of brain pathology.

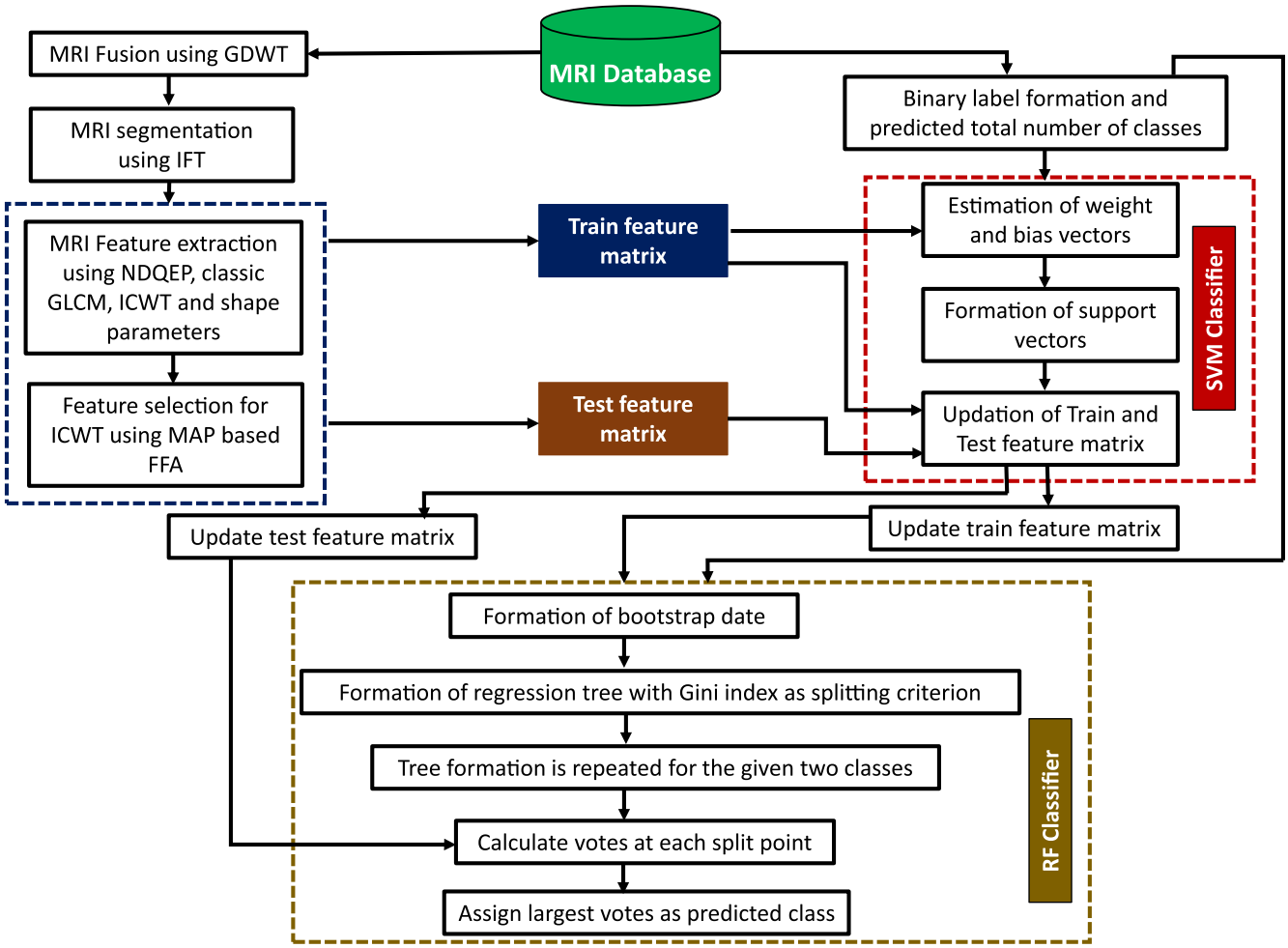

FIGURE 3. Flow diagram of the proposed classification approach.

F. CLASSIFICATION APPROACH USING HYBRIDIZED SUPPORT VECTOR BASED FOREST CLASSIFIER (HSVFC)

The Classification is the process of classifying the images based on the trained features. Generally the level or grade of the tumor and stroke can be determined by applying the classification technique [43].

Here, the process of classification is performed based on the combination of Support Vector Machine (SVM) and the Random Forest classifier which is represented in figure 3. The dataset is comprised of different levels of tumor images (High-Grade and Low-Grade) and various types of stroke images (Sub-Acute and Acute) based on which binary labeling (L) is done separately for tumor (High-Grade-1; Low-Grade-0) and stroke (Sub-Acute-1; Acute-0) images.

The total number of classes (CL) are predicted by considering the same values in the formed label (L) without repetitions ($CL = 2$ for tumor and $CL = 2$ for stroke). Initially, SVM (binary) classifier is trained with dataset features and the formed label (L), from which the weight vector is calculated using Lagrange multipliers and it is given by,

$$W_k(t_f) = \lim_{k \to 1 \text{ to } CL} \lim_{t_f \to 1 \text{ to } FD} \sum_{o=1}^{I_{Tr}} \alpha(o) * L(o) * Train_{fes}[o, t_f] \tag{14}$$

here,W_k is the weight vector of each class, α is a vector of Lagrange Multiplier, which varies from 0 to 0.5 for I_{Tr}, I_{Tr} depicts the total number of tumor or stroke images (that are to be trained), $Train_{fea}$ signifies the input dataset features in matrix form, FD denotes the indices from 1 to a total number of extracted features (i.e. 61).

After this, the bias is estimated which separates the two classes and is given by,

$$B_k(t_f) = \frac{1}{I_{Tr}} \lim_{k \to 1 \text{ to } CL} \lim_{t_f \to 1 \text{to } FD} \times \sum_{o=1}^{T_r} (L(o) - Train_{fea}[o, t_f] * W_k(t_f)) \tag{15}$$

where, B_k is the bias vector of each class with the dimension of extracted features. From the estimated bias and weight vector, the support vectors (SV) are formed which helps to determine the appropriate margins among two classes and is given by,

$$SV_k(t_f) = \lim_{t_f \to 1 \text{ to } FD} \left(\frac{-B_k(t_f)}{W_k(t_f)} \right) \tag{16}$$

The train features and the test features are updated using hyperparameters such as scale factor (S_2) and shift (S_1) from the formed support vectors and is denoted as,

$$Train_{fea}[o, t_f] = \lim_{o \to 1 \text{to } I_{Tr}} \lim_{t_f \to 1 \text{to } FD} (S_2(t_f) * Train_{fea}[o, t_f] + s_1(t_f)) \tag{17}$$

$$Test_{fea}[u, t_f] = \lim_{u \to 1 \text{to } I_{Te}} \lim_{t_f \to 1 \text{to } FD} (S_2(t_f) * Test_{fea}[u, t_f] + s_1(t_f)) \tag{18}$$

where I_{Te} represents the total number of tumor or stroke images that are to be tested, $Test_{fea}$ indicates the features for testing images, $s_1$is calculated by the mean of support vectors, and s_2 is calculated by taking the inverse of the standard deviation of support vectors. The updated train features and the formed label (L) are given as input to the random forest algorithm for regression tree formation. In the RF algorithm, bootstrapping is done initially, in which Q number of features are selected randomly from the given updated train features for forming the decision trees. The Gini index (G) is considered as the splitting criterion at each node of the tree and given by,

$$Gini_p = 1 - \sum_{ab=1}^{CL} (P_{ab})^2 \tag{19}$$

where P_{ab} represents the probability of ab^{th} class in the Q features associated at the parent node (p) and $P_{ab} = \frac{M^{ab}}{N}$, M^{ab} indicates the number of features in ab^{th} class among Q features and N signifies the total number of Q features.

Similarly, splitting criteria for the left and the right node from the parent node are given by,

$$Gini_{split} = \frac{N_1}{N} Gini_{t_1} + \frac{N_2}{N} Gini_{t_2} \tag{20}$$

where N_1 and N_2 imply the number of features at node t_1 and t_2, i.e., left and right node. The Gini index value must be minimum, and it ranges from 0 to 1. The node splitting in the tree continues until the value of Gini index is zero. The tree formation is repeated for the given two classes. Moreover, the hyperparameters used for the RF classifier include an 'out-of-bag error prediction (OOBPred)', 'minleafsize' (minimum number of observations per leaf). The condition for OOBPred is 'ON' and the value of 'minleafsize' is 1. Thus, the RF classifier is trained with the updated train features to classify the updated test features. After tree formation, the votes f at each formed decision tree is calculated as,

$$\hat{f}_k(u) = \lim_{k \to 1 \text{ to } CL} \lim_{u \to 1 \text{to } I_{Te}} \lim_{t_f \to 1 \text{to } FD} \{f_k(Test_{fea}[u, t_f])\} \tag{21}$$

where f_k denotes the decision tree at each class

$$class(u) = \lim_{u \to 1 \text{to } I_{Te}} \left(\arg \max_{k \to 1 \text{to } CL} (\hat{f}_k(u)) \right) \tag{22}$$

The equation (22) represents the predicted class (high-grade, low-grade, sub-acute and acute) for all the given test features. It is done by selecting the class label which is having maximum vote values.

IV. EXPERIMENTAL RESULTS AND DISCUSSION

In this work, MRI brain images from BRATS (Brain Tumor Segmentation) 2013 [44] and ISLES (Ischemic Stroke Lesion Segmentation) [45] databases of having the image resolution of 96 dpi is used for brain pathology classification. The MRI brain tumor image dataset is obtained from BRATS 2013 challenges.[1] The MRI brain stroke image dataset is obtained from ISLES 2015 challenges.[2]

The dataset of a tumor consists of low-grade and high-grade patients, whereas the stroke dataset includes sub-acute and acute patients. Each low-grade and high-grade tumor patient has the MRI image sequences of T2-w, T1-w, T1-c, FLAIR, and each sub-acute stroke patient has the sequences like T2-w, T1-w, DWI, FLAIR whereas each acute stroke patient has the sequences like T2-w, T1-w, and DWI. In this present work, 1100 image samples (or patients) are considered for each MRI sequence (among which 600 samples are tumor affected images and 500 samples are stroke affected images) i.e., around 4,150 images are taken for experimentation. The Ground Truth (GT) images are taken from the same BRATS 2013 and ISLES 2015 database, which is used for the calculation of performance metrics.

As for computing, we have used the Desktop personal computer which has intel® core™ i5-6200U CPU running at 2.40 GHz using 4 GB of RAM, operating in the Windows 10 platform. MATLAB 2019b is used to implement the proposed methodology.

A. GRAPHICAL USER INTERFACE (GUI) IMPLEMENTATION

The experimental results are obtained by implementing GUI in MATLAB 2019b platform. The following steps were involved:

- **Step1.** Selection of input image.
- **Step2.** Pathology detection as tumor or stroke using KNN algorithm [38].
- **Step3.** Segmentation of image using IFT algorithm. It is carried out for both individual MRI sequences and for fused images which are obtained using the GDWT algorithm [38].
- **Step4.** Feature extraction using NDQEP, GLCM, and shape-based extraction, and ICWT. Feature selection for ICWT features using MFFA.
- **Step5.** Classification of MRI images as high-grade or low-grade tumor, sub-acute or acute stroke using HSVFC.

[1]https://www.smir.ch/BRATS/Start2013
[2]https://www.smir.ch/ISLES/Start2015

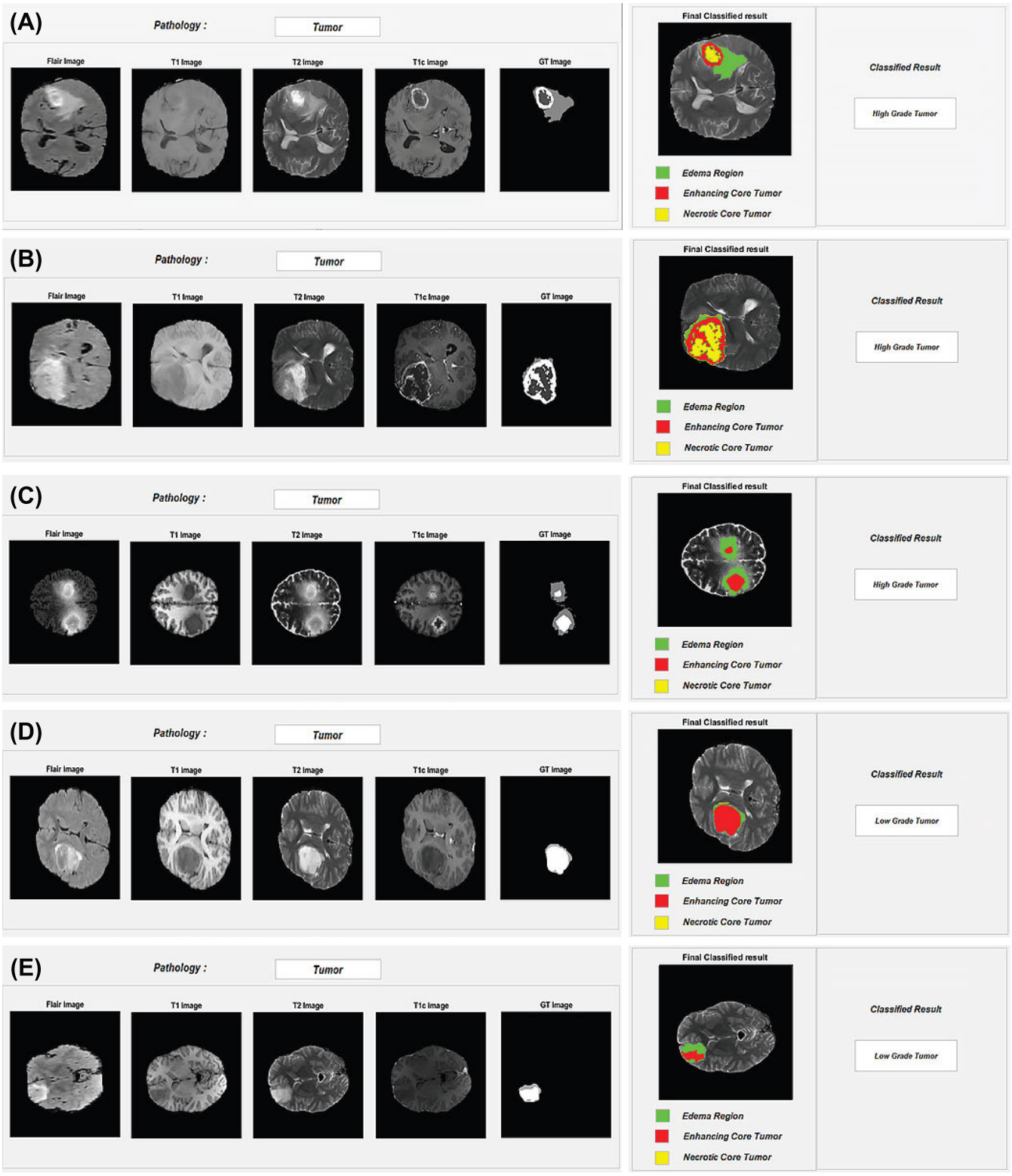

FIGURE 4. Input MRI sequences and classification output for brain tumor image of: (A) patient no.1, slice no.95; (B) patient no.14, slice no.95; (C) patient no.4, slice no.109; (D) patient no.6, slice no.143; and (E) patient no.10, slice no.77.

Step6. Performance analysis of different classifiers to prove the efficiency of the proposed classifier.

The classification results for MRI brain tumor images of patient no. 1, slice no. 95, and patient no. 14, slice no. 95 is shown in figure 4(A) and figure 4(B). The proposed HSVFC algorithm appropriately classifies the given MRI input as a high-grade tumor; besides, three different affected regions are identified such as edema, enhancing core tumor, and necrotic

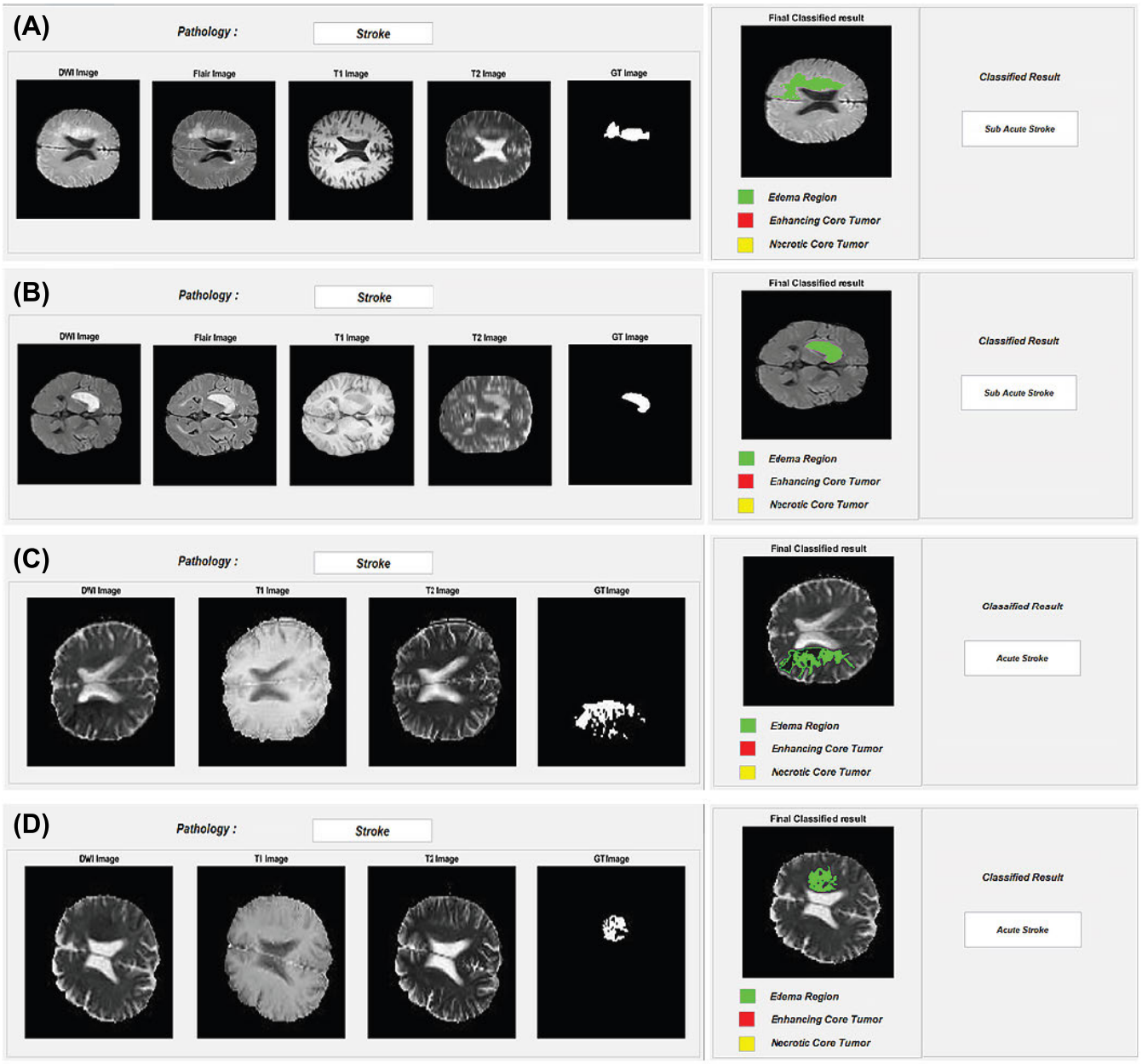

FIGURE 5. **Input MRI sequences and classification output for brain tumor image of: (A) patient no.8, slice no.96; (B) patient no.15, slice no.81; (C) patient no.16, slice no.46; and (D) patient no.8, slice no.42.**

tumor core based on the segmented result. figure 4(C) depicts the high-grade tumor classified result of patient no.4, slice no.109. Here, two tumors are predicted with two different regions such as edema and enhancing core tumor. Figure 4(D) and figure 4(E) represent the low-grade tumor classified results of patient no. 6, slice no. 143 and patient no.10, slice no.77. Edema and enhancing tumor core are identified as like in-ground truth images and highlighted with different colors. For patient no.8, slice no.96 and patient no.15, slice no.81, patient no. 16, slice no. 46 and patient no.8, slice no.42, the proposed classifier pertinently classifies the given MRI stroke input as sub-acute and acute case as shown in figure 5(A), 5(B), 5(C), and 5(D). The sub-acute stroke region is identified from the segmented output of DWI and FLAIR fused MRI, whereas acute stroke is known from a segmented result of DWI MRI and it is emphasized with green color.

In this work, we have tested the classifiers with five different training and testing ratios as 50-50, 60-40, 70-30, 80-20, and 90-10 and the accuracy of all these ratios has been presented in this section. The summary statistics of extracted features and its distributions over different classes are depicted in Table 1. Table 2 illustrates the accuracy of different features when the train-test ratio is 70-30. From the tabulated results it is understood that better accuracy

TABLE 1. Summary statistics of extracted features.

Methodology	Distribution of features
NDQEP	34
GLCM	20
Shape features	05
ICWT + MFFA	02
All*	61

*NDQEP + GLCM + Shape + (ICWT + MFFA)

TABLE 2. Accuracy measure of texture, shape and intensity features.

Methodology	Accuracy in(%)	
NDQEP	60.11	66.27
GLCM	49.28	50.34
Shape features	48.08	50.94
ICWT+ MFFA	58.66	62.81
All*	80.00	98.67

*NDQEP + GLCM + Shape + (ICWT + MFFA)

is achieved by combining the texture, intensity, and shape features compared to individual features.

To assess the performance of the proposed hybridized classifier (HSVFC), we compared its performance with the state-of-the-art classifiers such as K-Nearest Neighbor (KNN), Discriminant Classifier (DC), Feed Forward Neural Network (FFNN), Residual Network-18 (ResNet-18), and SVM. The performance measures to evaluate the proposed method include accuracy, precision, recall, F-score, False Positive Rate (FPR), and Jaccard.

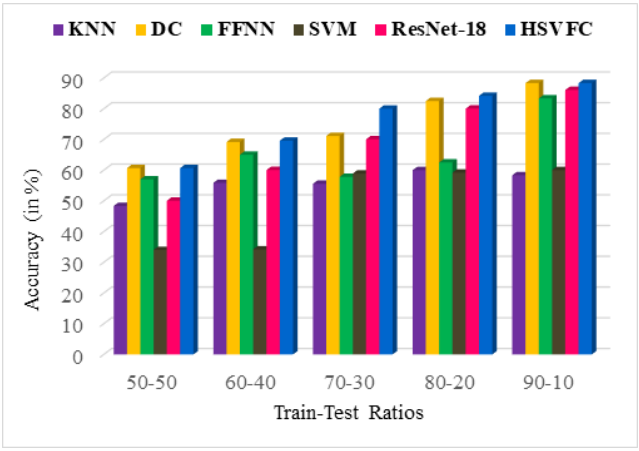

FIGURE 6. Accuracy measure of various classifiers for MRI brain tumor detection.

In figure 6, the highest mean accuracy of about 88.33% is obtained for HSVFC and DC algorithm when the train-test ratio is 90-10 and the lowest mean accuracy of 34% is obtained for SVM when the train-test ratio is 50-50 with respect to MRI brain tumor. Accuracy analysis concerning different train and test ratios for MRI brain stroke is shown in figure 7. The preferred accuracy value of 99.2% is achieved for the proposed HSVFC algorithm compared to other traditional classifiers even if the training data size is decreased and the testing data size is increased (50-50). Regardless of

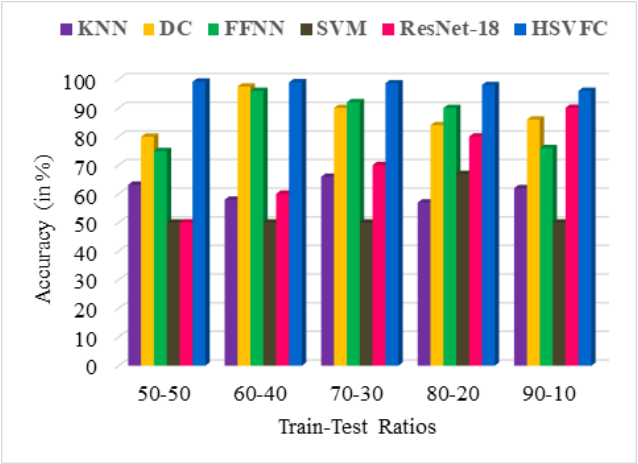

FIGURE 7. Accuracy measure of various classifiers for MRI brain stroke detection.

the train-test ratio, the performance of the proposed classifier seems to be loftier than the other conventional classifiers, since it is not necessary to do the training process repeatedly as like in other traditional classifiers to check the occurrence of error and also we have found support vectors alone from SVM which is given as input for the random forest to avoid the overfitting and frequent tuning of hyperparameter during the training process is not necessary. Further, the collection of features using our proposed techniques makes the proposed HSVFC classify the results in a better manner. The least accuracy of 50% is attained for the SVM classifier because it is prone to overfitting. For all the remaining conventional classifiers, such as KNN, DC, and ResNet-18 it is necessary to do the training process repeatedly which is a major drawback. However, the FFNN classifier also prone to overfitting and the convergence rate is large.

The most reliable and acceptable training and the testing ratio of 70-30 and 60-40 are considered for more detailed investigation about the performance measure and is discussed in the following section.

B. RESULT ANALYSIS OF PROPOSED HSVFC FOR 70-30 AS TRAIN AND TEST RATIO

In figure 8, it is understood that the value of recall (0.80), precision (0.94), F-score (0.86), and Jaccard (0.76) seems to be high and the value of FPR (0.18) is low for the proposed classifier compared to others in detecting high-grade tumors from MRI images. Next to the proposed HSVFC algorithm, DC is performing better. The concert of KNN and SVM classifier goes hand in hand. Further, the recital measures of ResNet-18 are found to be low compared to the proposed HSVFC and DC, but they are found to be high compared to KNN, FFNN, and SVM.

In figure 9, a high value of F-score (0.63) is attained for HSVFC, since it has low false positive and false negative values compared to others. The FPR (0.34) is high for KNN but low for ResNet-18 (0.18). A high Jaccard index value (0.46)

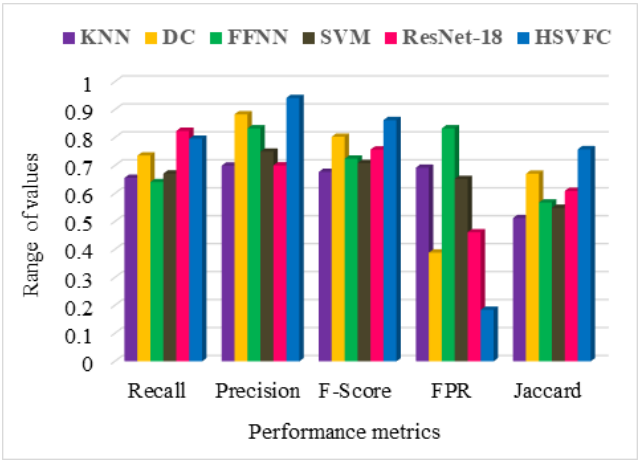

FIGURE 8. Performance measures of various classifiers in brain high-grade tumor detection.

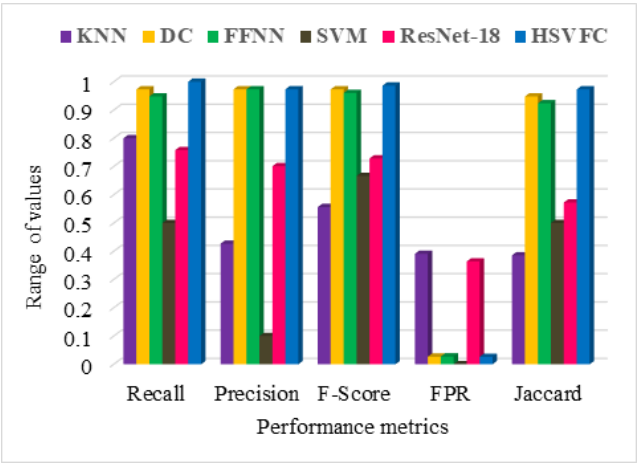

FIGURE 10. Performance measures of various classifier in MRI brain sub-acute stroke detection.

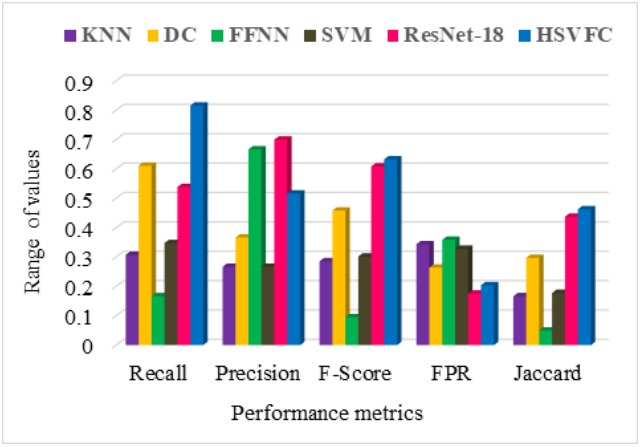

FIGURE 9. Performance measures of various classifiers in brain low-grade tumor detection.

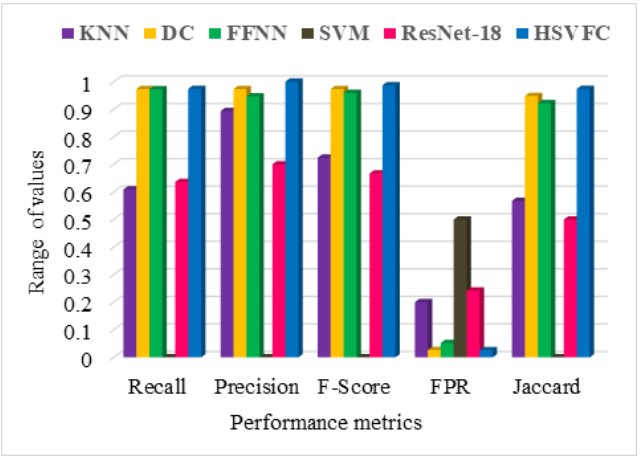

FIGURE 11. Performance measures of various classifiers in MRI brain acute stroke detection.

is observed for the proposed HSVFC and a low (0.05) for FFNN. The ResNet-18 classifier performs better than KNN, DC, FFNN, and SVM classifiers, but its performance is observed inferior to the proposed HSVFC.

The comparative analysis of various classifiers for MRI brain sub-acute stroke is depicted in figure 10. The best recall (1.00) and F-score (0.98) is achieved for the proposed classifier, whereas SVM has the least recall (0.5) measure and KNN has the poor F-score (0.55). The FPR is zero for SVM and 0.02 for HSVFC. The highest Jaccard index value (0.97) is achieved for the proposed HSVFC. The recital measures of DC and FFNN classifiers concord with each other. Likewise, the performance of the KNN classifier and ResNet-18 model goes hand in hand.

The concert measures for MRI brain acute stroke are depicted in figure 11. For DC and FFNN algorithm, the range of performance metrics gets along with each other. The least FPR of 0.02, high Jaccard index of 0.97, and high F-score of 0.98 are obtained for the proposed HSVFC. The F-score and Jaccard index look similar for the KNN and ResNet-18 algorithms.

C. RESULT ANALYSIS OF PROPOSED HSVFC FOR 60-40 AS TRAIN AND TEST RATIO

In the case of testing, the proposed HSVFC with 60% training and 40% testing data, the range of F-score varies from 0.31 to 0.81 for all the classifiers in brain tumors detection as shown in figure 12. Among the F score, the highest score (0.81) is accomplished by the proposed classifier, besides, the recall (0.75) and precision (0.98) rates are high. The utmost Jaccard index (0.68) is obtained for the proposed HSVFC. The false-positive rate (0.23) is low for HSVFC and high (0.66) for KNN. For DC and FFNN, the FPR concords with each other. The F-score of ResNet-18 is 18% low compared to HSVFC.

In figure 13, the recall value of 0.79, precision rate of 0.12, F-score of 0.50, FPR of 0.23, and Jaccard index of 0.33 are attained for HSVFC in low-grade tumor detection. Next to the proposed HSVFC, the ResNet-18 method performs well.

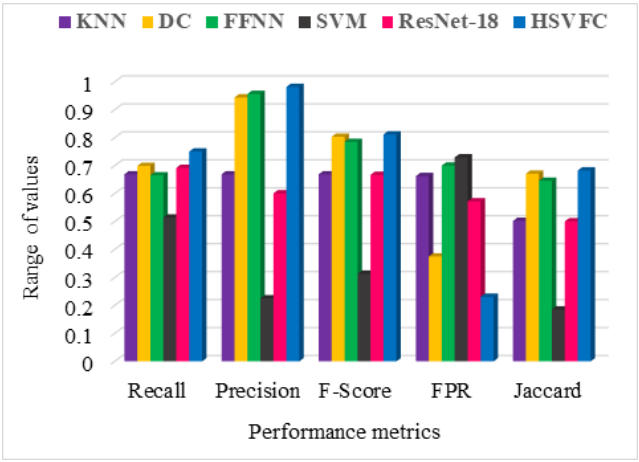

FIGURE 12. Performance measures of various classifiers in MRI brain high-grade tumor detection.

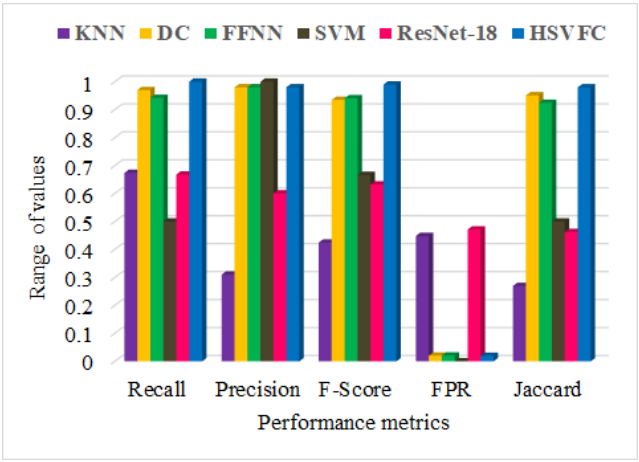

FIGURE 14. Performance measures of various classifiers in MRI brain sub-acute stroke detection.

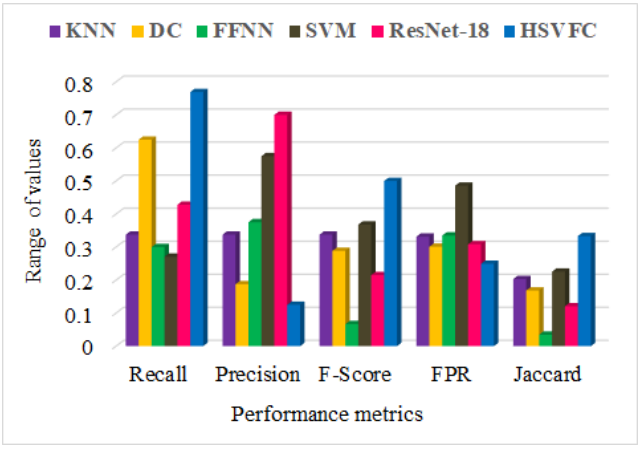

FIGURE 13. Performance measures of various classifiers in MRI brain low-grade tumor detection.

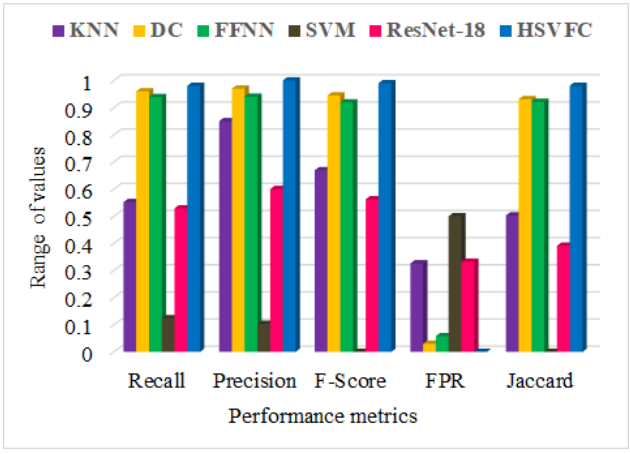

FIGURE 15. Performance measures of various classifiers in MRI brain sub-acute stroke detection.

Unique performance metric values are accomplished for each classifier. Poor performance is observed for KNN, by having the least recall, precision, and F-score, and high FPR.

The result analysis of different classifiers in brain sub-acute and acute stroke detection is shown in figure 14 and figure 15. For both sub-acute and acute stroke, the performance of DC and FFNN agrees with each other. The small F-score is perceived for the KNN algorithm, whereas the perfect F-score of 0.99 is achieved for HSVFC for both sub-acute and acute stroke. The FPR is zero for HSVFC in the case of acute stroke, and 0.02 for sub-acute stroke.

D. RESULT ANALYSIS OF PROPOSED HSVFC USING CONFUSION MATRIX AND RECEIVER OPERATING CURVE (ROC)

The total number of tumor images for each MRI sequence considered in this work is 600, amongst which 400 images belong to the High-Grade (HG) class and the remaining 200 images are the Low-Grade (LG).

TABLE 3. Confusion matrix of HSVFC for tumor detection (70-30 as train-test ratio). TP: True Positive; TN: True Negative, FP: False Positive, FN: False Negative.

	Predicted values	
Actual values	TP=113 (HG) TP=31 (LG)	FN=29 (HG) FN=7 (LG)
	FP=7 (HG) FP=29 (LG)	TN=31 (HG) TN=113 (LG)

In Table 3, 70% of the images are considered for training, which means that 280 HG and 140 LG tumor images are reviewed for training. For the testing process, 30% of the tumor images are considered, which implies 120 HG tumor images and 60 LG tumor images are taken for testing. The results in the confusion matrix show that, of the 120 HG tumor images, around 113 images are predicted correctly (i.e, positive cases) and among 60 LG tumor images, 31 images are projected as positive cases. The total number of stroke images for each MRI sequence considered in this work is 500, amongst which 250 images belong to Sub-Acute (AC)

TABLE 4. Confusion matrix of HSVFC for stroke detection (70-30 as train-test ratio). TP: True Positive; TN: True Negative, FP: False Positive, FN: False Negative.

	Predicted values	
Actual values	TP=73 (SA) TP=75 (A)	FN=0 (SA) FN=2 (A)
	FP=2 (SA) FP=0 (A)	TN=75 (SA) TN=73 (A)

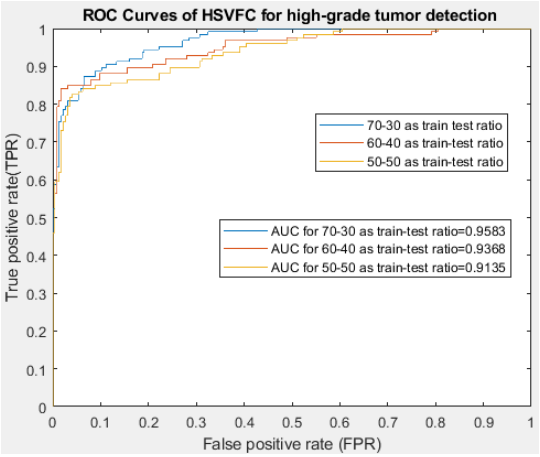

FIGURE 16. ROC of HSVFC for MRI brain high-grade tumor detection.

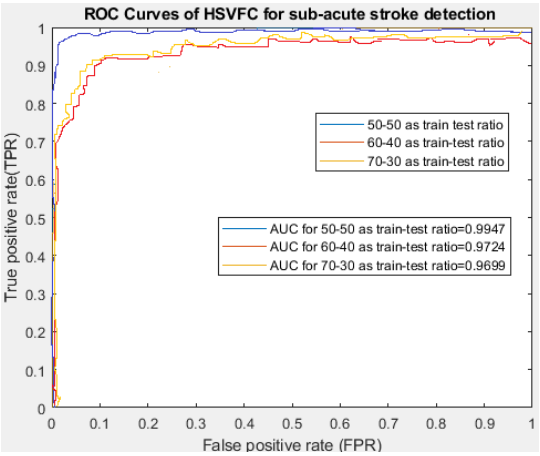

FIGURE 17. ROC of HSVFC for MRI brain sub-acute stroke detection.

class and the remaining 250 images are Acute (A). In Table 4, 70% of the images are considered for training, which means that 175-SA and 175-acute tumor images are reviewed for training. For the testing process, 30% of the stroke images are considered, which implies 75 SA and 75 acute stroke images are taken for testing. The results in the confusion matrix show that, of the 75 SA stroke images, around 73 images are predicted correctly (i.e, positive cases) and among 75 acute stroke images, all the 75 images are projected as positive cases.

In figure 16, for high-grade tumor class detection, the high value of Area Under the Curve (AUC-0.95) is obtained for the proposed HSVFC when the train-test ratio is 70-30. Similarly, for sub-acute stroke detection, the high value of Area Under the Curve (AUC-0.99) is obtained for the proposed HSVFC when the train-test ratio is 50-50 (figure 17). The proposed work is not suitable for large databases (i.e., for multiple images with different pathological condition) which is considered as the major limitation.

V. CONCLUSION AND FUTURE WORK

This paper describes a hybridized classification technique by combining support vector machine and random forest methods for detecting tumor and stroke in the brain MRI's. Also, NDQEP and ICWT are proposed for feature extraction and MFFA is projected for feature selection technique to augment the classification process. By using the proposed HSVFC method, MRI brain tumor images are detected and classified as low-grade tumors and high-grade tumors. Similarly, MRI brain stroke images are detected and classified as acute stroke and sub-acute stroke. In tumor detection, three different regions such as edema, necrotic tumor core, and non-enhancing tumor core region are identified and emphasized with different colors. The experimental analysis offers the results in such a way that, for MRI brain tumor classification, the average accuracy of HSVFC is prominent than SVM by 43.42%, FFNN by 16.13%, DC by 2.90%, ResNet-18 by 10.01%, and KNN by 31.68%. Similarly, for MRI brain stroke classification, the average accuracy of HSVFC is greater than SVM by 53.40%, FFNN by 13.45%, DC by 11.49%, ResNet-18 by 33.42%, and KNN by 46.33%. For the proposed HSVFC, the best F-score of 0.91 and the least FPR of 0.06 are attained concerning MRI brain tumor classification. Likewise, HSVFC accomplishes 0.99 as the best F-score and FPR as 0 in the case of MRI brain stroke classification. Deep neural networks can be utilized in the future for detecting multiple brain diseases by collecting the input images from several databases without applying data augmentation to achieve high accuracy and low error in predicting the diseases.

CONFLICT OF INTEREST

The authors declare no conflict of interest.

REFERENCES

[1] Y. Xu, Z. Jia, Y. Ai, F. Zhang, M. Lai, I. Eric, and C. Chang, "Deep convolutional activation features for large scale brain tumor histopathology image classification and segmentation," in *Proc. ICASSP*, Apr. 2015, pp. 947–951.

[2] G. Praveen and A. Agrawal, "Hybrid approach for brain tumor detection and classification in magnetic resonance images," in *Proc. CCIS*, 2015, pp. 162–166.

[3] J. Hu, W.-S. Pang, J. Han, K. Zhang, J.-Z. Zhang, and L.-D. Chen, "Gualou Guizhi decoction reverses brain damage with cerebral ischemic stroke, multi-component directed multi-target to screen calcium-overload inhibitors using combination of molecular docking and protein–protein docking," *J. Enzyme Inhibition Medicinal Chem.*, vol. 33, no. 1, pp. 115–125, Jan. 2018.

[4] A. M. Hasan, H. A. Jalab, F. Meziane, H. Kahtan, and A. S. Al-Ahmad, "Combining deep and handcrafted image features for MRI brain scan classification," *IEEE Access*, vol. 7, pp. 79959–79967, 2019.

[5] R. A. Zeineldin, M. E. Karar, J. Coburger, C. R. Wirtz, and O. Burgert, "DeepSeg: Deep neural network framework for automatic brain tumor segmentation using magnetic resonance FLAIR images," *Int. J. Comput. Assist. Radiol. Surg.*, vol. 15, no. 6, pp. 909–920, Jun. 2020.

[6] M. A. Queiroz, M. Hüllner, F. Kuhn, G. Huber, C. Meerwein, S. Kollias, G. von Schulthess, and P. Veit-Haibach, "Use of diffusion-weighted imaging (DWI) in PET/MRI for head and neck cancer evaluation," *Eur. J. Nucl. Med. Mol. Imag.*, vol. 41, no. 12, pp. 2212–2221, Dec. 2014.

[7] L. Ali, A. Hussain, J. Li, A. Shah, U. Sudhakr, M. Mahmud, U. Zakir, X. Yan, B. Luo, and M. Rajak, "Intelligent image processing techniques for cancer progression detection, recognition and prediction in the human liver," in *Proc. CICARE*, 2014, pp. 25–31.

[8] M. Mahmud, M. S. Kaiser, A. Hussain, and S. Vassanelli, "Applications of deep learning and reinforcement learning to biological data," *IEEE Trans. Neural Netw. Learn. Syst.*, vol. 29, no. 6, pp. 2063–2079, Jun. 2018.

[9] H. M. Ali, M. S. Kaiser, and M. Mahmud, "Application of convolutional neural network in segmenting brain regions from MRI data," in *Brain Informatics*. Cham, Switzerland: Springer, 2019, pp. 136–146.

[10] M. B. T. Noor, N. Z. Zenia, M. S. Kaiser, M. Mahmud, and S. Al Mamun, "Detecting neurodegenerative disease from MRI: A brief review on a deep learning perspective," in *Brain Informatics*. Cham, Switzerland: Springer, 2019, pp. 115–125.

[11] M. Mahmud, M. S. Kaiser, and A. Hussain, "Deep learning in mining biological data," *Cogn. Comput.*, vol. 13, no. 1, pp. 1–33, Jan. 2021.

[12] M. B. T. Noor, N. Z. Zenia, M. S. Kaiser, S. A. Mamun, and M. Mahmud, "Application of deep learning in detecting neurological disorders from magnetic resonance images: A survey on the detection of Alzheimer's disease, Parkinson's disease and schizophrenia," *Brain Informat.*, vol. 7, no. 1, pp. 1–21, Dec. 2020.

[13] V. M. Aradhya, M. Mahmud, D. Guru, B. Agarwal, and M. S. Kaiser, "One-shot cluster-based approach for the detection of COVID-19 from chest X-ray images," *Cogn. Comput.*, vol. 13, no. 4, pp. 873–881, Jul. 2021.

[14] N. Dey, V. Rajinikanth, S. J. Fong, M. S. Kaiser, and M. Mahmud, "Social group optimization–assisted Kapur's entropy and morphological segmentation for automated detection of COVID-19 infection from computed tomography images," *Cogn. Comput.*, vol. 12, no. 5, pp. 1011–1023, 2020.

[15] Y. Miah, C. N. E. Prima, S. J. Seema, M. Mahmud, and M. S. Kaiser, "Performance comparison of machine learning techniques in identifying dementia from open access clinical datasets," in *Proc. ICACIn*, 2021, pp. 79–89, doi: 10.1007/s12559-021-09848-3.

[16] A. K. Singh, A. Kumar, M. Mahmud, M. S. Kaiser, and A. Kishore, "COVID-19 infection detection from chest X-ray images using hybrid social group optimization and support vector classifier," *Cognit. Comput.*, pp. 1–13, Mar. 2021, doi: 10.1007/s12559-021-09848-3.

[17] R. V. Tali, S. Borra, and M. Mahmud, "Detection and classification of leukocytes in blood smear images: State of the art and challenges," *Int. J. Ambient Comput. Intell.*, vol. 12, no. 2, pp. 111–139, Apr. 2021.

[18] N. A. B. Mary and D. Dharma, "Coral reef image classification employing improved LDP for feature extraction," *J. Vis. Commun. Image Represent.*, vol. 49, pp. 225–242, Nov. 2017.

[19] O. Maier, C. Schröder, N. D. Forkert, T. Martinetz, and H. Handels, "Classifiers for ischemic stroke lesion segmentation: A comparison study," *PLoS ONE*, vol. 10, no. 12, Dec. 2015, Art. no. e0145118.

[20] B. Deepa and M. Sumithra, "A new amalgam technique in cad system for detection of abnormality in MRI brain images," *Adv. Nat. Appl. Sci.*, vol. 10, no. 4, pp. 95–104, 2016.

[21] K. Usman and K. Rajpoot, "Brain tumor classification from multimodality MRI using wavelets and machine learning," *Pattern Anal. Appl.*, vol. 20, no. 3, pp. 871–881, 2017.

[22] N. M. Saad, N. Noor, A. Abdullah, S. Muda, A. Muda, and N. A. Rahman, "Automated stroke lesion detection and diagnosis system," in *Proc. Int. Multiconf. Eng. Comput. Sci.*, vol. 1, 2017, pp. 1–6.

[23] H. Lee, E.-J. Lee, S. Ham, H.-B. Lee, J. S. Lee, S. U. Kwon, J. S. Kim, N. Kim, and D.-W. Kang, "Machine learning approach to identify stroke within 4.5 hours," *Stroke*, vol. 51, no. 3, pp. 860–866, Mar. 2020.

[24] J. Amin, M. Sharif, M. Yasmin, and S. L. Fernandes, "A distinctive approach in brain tumor detection and classification using MRI," *Pattern Recognit. Lett.*, vol. 139, pp. 118–127, Nov. 2020.

[25] G. Deep, L. Kaur, and S. Gupta, "Directional local ternary quantized extrema pattern: A new descriptor for biomedical image indexing and retrieval," *Eng. Sci. Technol., Int. J.*, vol. 19, no. 4, pp. 1895–1909, Dec. 2016.

[26] G. Jothi, "Hybrid tolerance rough set–firefly based supervised feature selection for MRI brain tumor image classification," *Appl. Soft Comput.*, vol. 46, pp. 639–651, Sep. 2016.

[27] M. Soltaninejad, L. Zhang, T. Lambrou, G. Yang, N. Allinson, and X. Ye, "MRI brain tumor segmentation and patient survival prediction using random forests and fully convolutional networks," in *Proc. Int. MICCAI Brainlesion Workshop*, 2017, pp. 204–215.

[28] A. Shenbagarajan, V. Ramalingam, C. Balasubramanian, and S. Palanivel, "Tumor diagnosis in MRI brain image using ACM segmentation and ANN-LM classification techniques," *Indian J. Sci. Technol.*, vol. 9, no. 1, pp. 1–12, Feb. 2016.

[29] K. Machhale, H. B. Nandpuru, V. Kapur, and L. Kosta, "MRI brain cancer classification using hybrid classifier (SVM-KNN)," in *Proc. ICIC*, 2015, pp. 60–65.

[30] T. Gupta, T. K. Gandhi, R. K. Gupta, and B. K. Panigrahi, "Classification of patients with tumor using MR FLAIR images," *Pattern Recognit. Lett.*, vol. 139, pp. 112–117, Nov. 2020.

[31] T. Rajesh, R. S. M. Malar, and M. R. Geetha, "Brain tumor detection using optimisation classification based on rough set theory," *Cluster Comput.*, vol. 22, no. S6, pp. 13853–13859, Nov. 2019.

[32] J. C. Griffis, J. B. Allendorfer, and J. P. Szaflarski, "Voxel-based Gaussian naïve Bayes classification of ischemic stroke lesions in individual T1-weighted MRI Scans," *J. Neurosci. Methods*, vol. 257, pp. 97–108, Jan. 2016.

[33] J. Oh, S. Cha, A. H. Aiken, E. T. Han, J. C. Crane, J. A. Stainsby, G. A. Wright, W. P. Dillon, and S. J. Nelson, "Quantitative apparent diffusion coefficients and T2 relaxation times in characterizing contrast enhancing brain tumors and regions of peritumoral edema," *J. Magn. Reson. Imag.*, vol. 21, no. 6, pp. 701–708, 2005.

[34] M. Ambrosanio, F. Baselice, G. Ferraioli, F. Lenti, and V. Pascazio, "Intra voxel analysis in magnetic resonance imaging," *Magn. Reson. Imag.*, vol. 37, pp. 70–80, Apr. 2017.

[35] C. S. S. Anupama, M. Sivaram, E. L. Lydia, D. Gupta, and K. Shankar, "Synergic deep learning model–based automated detection and classification of brain intracranial hemorrhage images in wearable networks," *Pers. Ubiquitous Comput.*, pp. 1–10, Nov. 2020, doi: 10.1007/s00779-020-01492-2.

[36] A. Nayyar, S. Garg, D. Gupta, and A. Khanna, "Evolutionary computation: Theory and algorithms," in *Advances in Swarm Intelligence for Optimizing Problems in Computer Science*. Boca Raton, FL, USA: CRC Press, 2018, pp. 1–26.

[37] A. Khamparia, D. Gupta, V. H. C. de Albuquerque, A. K. Sangaiah, and R. H. Jhaveri, "Internet of health things-driven deep learning system for detection and classification of cervical cells using transfer learning," *J. Supercomput.*, vol. 76, pp. 8590–8608, Jan. 2020.

[38] B. Deepa and M. G. Sumithra, "An intensity factorized thresholding based segmentation technique with gradient discrete wavelet fusion for diagnosing stroke and tumor in brain MRI," *Multidimensional Syst. Signal Process.*, vol. 30, no. 4, pp. 2081–2112, Oct. 2019.

[39] R. Usha and K. Perumal, "SVM classification of brain images from MRI scans using morphological transformation and GLCM texture features," *Int. J. Comput. Syst. Eng.*, vol. 5, no. 1, pp. 18–23, 2019.

[40] K. Devi, P. Gupta, D. Grover, and A. Dhindsa, "An effective texture feature extraction approach for iris recognition system," in *Proc. ICACCA*, 2016, pp. 1–5.

[41] W. Ayadi, W. Elhamzi, I. Charfi, B. Ouni, and M. Atri, "Brain MRI classification using discrete wavelet transform and bag-of-words," in *Proc. IC_ASET*, vol. 2018, pp. 45–49.

[42] M. A. Kabir, "Automatic brain tumor detection and feature extraction from MRI image," *Glob. Sci. J.*, vol. 8, no. 4, pp. 695–711, 2020.

[43] M. W. Nadeem, M. A. A. Ghamdi, M. Hussain, M. A. Khan, K. M. Khan, S. H. Almotiri, and S. A. Butt, "Brain tumor analysis empowered with deep learning: A review, taxonomy, and future challenges," *Brain Sci.*, vol. 10, no. 2, p. 118, Feb. 2020.

[44] B. H. Menze *et al.*, "The multimodal brain tumor image segmentation benchmark (BRATS)," *IEEE Trans. Med. Imag.*, vol. 34, no. 10, pp. 1993–2024, Oct. 2015.

[45] O. Maier, B. H. Menze, J. von der Gablentz, L. Häni, M. P. Heinrich, M. Liebrand, S. Winzeck, A. Basit, P. Bentley, and L. Chen, "ISLES 2015—A public evaluation benchmark for ischemic stroke lesion segmentation from multispectral MRI," *Med. Image Anal.*, vol. 35, pp. 250–269, Jan. 2017.

B. DEEPA received the B.E. degree in electronics and communication engineering and the M.E. degree in communication engineering from the Bannari Amman Institute of Technology, Sathyamangalam, Erode, India, in 2009 and 2011, respectively. She is currently pursuing the Ph.D. degree in information and communication engineering with Anna University, Chennai. She is also working as an Assistant Professor with the Department of Electronics and Communication Engineering, Jayaram College of Engineering and Technology, Tiruchirappalli, India. She has published 12 technical articles in refereed journals, 16 research articles in national and international conferences in India and abroad. Her research interests include signal/image processing, biomedical engineering, and wireless communications.

M. MURUGAPPAN (Senior Member, IEEE) received the Ph.D. degree in mechatronic engineering from Universiti Malaysia Perlis, Malaysia, in 2010. Since February 2016, he has been an Associate Professor with the Department of Electronics and Communication Engineering, Kuwait College of Science and Technology (KCST) (Private University), Kuwait. He has gained more than ten years of post-Ph.D. teaching and research experience from different countries (India, Malaysia, and Kuwait). Recently, he has been included in the top 2% of scientist in the world in experimental psychology and artificial intelligence by Stanford University researchers. He has published more than 110 research articles in peer-reviewed conference proceedings/journals/book chapters. He has got a maximum citation of 3900 and the H-index of 33 and i10 index of 66 (Ref: Google Scholar citations). He secured nearly $2.5 Million as research grants from the Government of Malaysia, Malaysia, and Kuwait Foundation for Advancement of Sciences (KFAS), Kuwait for continuing his research works and successfully guided 14 postgraduate students (9 Ph.D. and 5 M.Sc.). His research interests include affective computing, the Internet of Things (IoT), the Internet of Medical Things (IoMT), cognitive neuroscience, brain–computer interface, neuromarketing, medical image processing, machine learning, and artificial intelligence. He has received several research awards, medals, and certificates on excellent publications and research products. He is also serving as a Chair for Educational Activities in the IEEE Kuwait Section. He is serving as an Editorial Board Member for *PLoS ONE*, *Journal of Medical Imaging and Health Informatics*, and *International Journal of Cognitive Informatics*.

M. G. SUMITHRA (Senior Member, IEEE) received the B.E. degree in electronics and communication engineering from the Government College of Engineering, Salem, India, in 1994, the M.E. degree in medical electronics from the College of Engineering, Guindy, Anna University, Chennai, India, in 2001, and the Ph.D. degree in information and communication engineering from Anna University, in 2011. She is currently working as a Professor of Electronics and Communication Engineering, Director of Centre for Research and Development and the Head of the Bio-Medical Engineering Department, Dr. N. G. P. Institute of Technology, Coimbatore, Tamil Nadu, India. She is having 25 years of teaching experience. She has published 78 technical articles in refereed journals, four book chapters, and 134 research papers in national and international conferences in India, and five abroad. In addition, she is an NVIDIA Deep Learning Institute Certified Instructor for ''Computer Vision.'' She is a Recognized Supervisor of Anna University, Chennai, and five research scholars are pursuing Ph.D. under her supervision and one awarded a Ph.D. degree. She has published seven patents. Her research interests include signal/image processing, biomedical engineering, wireless communications, and artificial intelligence. She is an Active Member in various professional societies, such as ISTE, IETE, and IET.

MUFTI MAHMUD (Senior Member, IEEE) received the Ph.D. degree in information engineering from the University of Padova, Italy, in 2011. He is currently working as an Associate Professor of computer science with Nottingham Trent University, U.K. With over 18 years of experience in the industry and academia in India, Bangladesh, Italy, Belgium, and U.K. He is an expert in computational intelligence, applied data analysis, and big data technologies with a keen focus on healthcare applications. He has published over 150 peer-reviewed articles and papers in leading journals and conferences, and (co-)edited five volumes and many journal special issues on those domains. He has secured research grants totaling a sum of approximately $3.3 million. He has supervised two postdoctoral and over 50 research students (Ph.D., master's, and bachelor's). He is also a Senior Member of ACM, a Professional Member of the British Computer Society, and a fellow of the Higher Education Academy, U.K. He was a recipient of the Vice-Chancellor's Outstanding Research Award 2020 at the NTU and the Marie-Curie Postdoctoral Fellowship, in 2013. From 2020 to 2021, he was the Vice-Chair of the Intelligent System Application and Brain Informatics Technical Committees of the IEEE Computational Intelligence Society (CIS), a member of the IEEE CIS Task Force on Intelligence Systems for Health, an Advisor of the IEEE R8 Humanitarian Activities Subcommittee, the Publications Chair of the IEEE UK and Ireland Industry Applications Chapter, and the Project Liaison Officer of the IEEE UK and Ireland SIGHT Committee. He has also served as the Coordinating Chair of the Local Organization of the IEEE-WCCI2020; the General Chair of BI2020, 2021, and AII2021; and the Program Chair of the IEEE-CICARE2020 and 2021. He serves as a Section Editor (Big Data Analytics) for the *Cognitive Computation* journal, an Associate Editor for the *Frontiers in Neuroscience*, and *Big Data Analytics* journals, and a Regional Editor (Europe) for the *Brain Informatics* journal.

MABROOK S. AL-RAKHAMI (Member, IEEE) received the master's degree in information systems from King Saud University, Riyadh, Saudi Arabia, where he is currently pursuing the Ph.D. degree with the Information Systems Department, College of Computer and Information Sciences. He worked as a Lecturer with King Saud University, Muzahimiyah Branch, where he taught many courses, such as programming languages in computer and information science. He has authored several articles in peer-reviewed IEEE/ACM/Springer/Wiley journals and conferences. His research interests include edge intelligence, social networks, cloud computing, the Internet of Things, big data, and health informatics.